Available online at www.sciencedirect.com
SCIENCE DIRECT®
Catalysis Today 116 (2006) 184–190
CATALYSIS TODAY
www.elsevier.com/locate/cattod

Acid site requirements for the synthesis of *o*-hydroxyacetophenone by acylation of phenol with acetic acid

C.L. Padró, M.E. Sad, C.R. Apesteguía *

Catalysis Science and Engineering Research Group (GICIC), Instituto de Investigaciones en Catálisis y Petroquímica -INCAPE-(UNL-CONICET), Santiago del Estero 2654, (3000) Santa Fe, Argentina

Available online 30 May 2006

Abstract

The acid site requirements for the synthesis of *o*-hydroxyacetophenone (*o*-HAP) by acylation of phenol with acetic acid were studied on samples containing only strong Brönsted (HPA/C) or Lewis (NaY) acid sites, and also on catalysts containing both Lewis and Brönsted acid sites of either strong (zeolite ZSM5) or moderate (Al-MCM-41) strength. The nature, density, and strength of surface acid sites were probed by temperature-programmed desorption of NH_3 coupled with infrared spectra of adsorbed pyridine. The direct synthesis of *o*-HAP by C-acylation of phenol was promoted only on samples containing Lewis sites. The initial *o*-HAP formation rate followed the order ZSM5 $\gg$ Al-MCM-41 $\cong$ NaY, probably because ZSM5 promoted at higher rates the generation of acylating agent CH_3CO^+ from acetic acid. *o*-HAP was also produced via a two-step reaction pathway involving the initial O-acylation of phenol to phenyl acetate and the consecutive transformation of phenyl acetate to *o*-HAP. This latter step greatly depended on the nature and strength of surface acid sites, and it was specifically investigated by feeding phenyl acetate alone or together with phenol. It was found that phenyl acetate is converted to *o*-HAP via a Fries rearrangement mechanism on very strong Brönsted acid sites, and through an intermolecular phenol/phenyl acetate acylation on samples containing both Brönsted and Lewis acid sites, such as Al-MCM-41 and ZSM5.

Keywords: Hydroxyacetophenone synthesis; Acid catalysis; Phenol acylation; Fine chemistry

1. Introduction

Ortho-hydroxyacetophenone (*o*-HAP) is a key intermediate for producing 4-hydroxycoumarin and warfarin, which are both used as anticoagulant drugs [1], and it has been also employed for obtaining flavonones [2,3]. Liquid-phase Fries rearrangement of phenyl acetate using Friedel-Crafts catalysts produces mainly *para*-hydroxyacetophenone (*p*-HAP) and minor amounts of *o*-HAP [3,4]. Acylation of phenol in liquid-phase using acid halides [5] or acid anhydrides [6] as acylating agents also produces mainly *p*-HAP, although changing the solvent polarity may change the isomer selectivity. In contrast, *o*-HAP is the main product when the Fries rearrangement of phenyl acetate is carried out on solid acids in gas-phase, but considerable amounts of phenolic byproducts take place and catalyst activity decline on stream is significant [7,8]. Better *o*-HAP selectivities has been reported via the vapor-phase acylation of phenol with acetic acid [9,10]; however, co-production of phenyl acetate is significant and catalysts are often deactivated because of coke formation.

Recently, we studied the gas-phase acylation of phenol with acetic acid over HPA-based catalysts, acid zeolites, and SiO_2-Al_2O_3 [11] with the aim of ascertaining the reaction mechanism leading to the formation of *o*-HAP on solid acids. We found that acid zeolites containing both strong Brönsted and Lewis acid sites produce *o*-HAP at high rates because efficiently catalyze the two main reaction pathways leading from phenol to *o*-HAP, i.e. the direct C-acylation of phenol and the O-acylation of phenol forming the phenyl acetate intermediate which is consecutively transformed via intermolecular phenol/phenyl acetate C-acylation. We also observed [11] that the *o*-HAP formation rate decreases on stream on all the solid acids employed excepting on zeolite ZSM5. Thus, we investigated the reaction on zeolites HY, HBeta, and ZSM5 to elucidate the catalyst deactivation mechanism and to ascertain the causes for

* Corresponding author. Tel.: +54 342 4555279; fax: +54 342 4531068.
E-mail address: capesteg@fiqus.unl.edu.ar (C.R. Apesteguía).
URL: http://www.ceride.gov.ar/gicic

0920-5861/$ – see front matter © 2006 Elsevier B.V. All rights reserved.
doi:10.1016/j.cattod.2006.01.029

the superior stability of zeolite ZSM5 on stream [12]. In this paper, we have extended these studies with the goal of establishing the exact requirements of surface acid site density and strength to promote the *o*-HAP synthesis. Specifically, we studied the gas-phase acylation of phenol with acetic acid on samples containing only either strong Brönsted (HPA/C) or Lewis (NaY) acid sites; catalysts containing both Lewis and Brönsted acid sites of either strong (zeolite ZSM5) or moderate (Al-MCM-41) strength were also used. Results will show that the primary and secondary reaction pathways leading from phenol to *o*-HAP greatly depend on the nature, density, and strength of surface acid sites that are probed by temperature-programmed desorption of NH_3 coupled with infrared spectra of adsorbed pyridine. The superior activity of zeolite ZSM5 for producing *o*-HAP is interpreted in terms of the relative abundance of strong Brönsted and Lewis acid sites required to both generate the acylating agent from acetic acid and acylate directly phenol in *ortho*-position.

2. Experimental

The H form of zeolite ZSM5 was prepared by triple ion exchange of a commercial Na-ZSM5 zeolite (Zeocat Pentasil PZ-2/54, Si/Al = 20) with ammonium acetate (Sigma, 99%) at 298 K and subsequent calcination in air at 773 K. Zeolite NaY was from UOP (UOP-Y 54, Si/Al = 2.4). HPA(28%)/C was prepared by stirring a suspension of Carbon (from Westvaco) in a hydrochloric HPA solution at pH 1.6 for 24 h. Mesoporous Al-MCM-41 of a Si/Al = 18 ratio was synthesized according to Edler and White [13]. Sodium silicate solution (14% NaOH and 27% SiO_2, Aldrich), cetyltrimethylammonium bromide (Aldrich), aluminum isopropoxide (Aldrich), and deionizated water were used as the reagents. The composition of the synthesis gel was $7SiO_2$-xAl_2O_3-$2.7Na_2O$-3.7CTMABr-$1000H_2O$. The pH was adjusted to 10 using a 1 M H_2SO_4 solution, then the gel was transferred to a Teflon lined stainless-steel autoclave and heated to 373 K in an oven for 96 h. After crystallization, the solid was washed with deionizated water, dried at 373 K and finally calcined at 773 K for 4 h.

BET surface areas (S_g), mean pore diameter ($\overline{d}_p$), and pore size distribution were measured by N_2 physisorption at its boiling point in a Quantochrome Corporation NOVA-1000 sorptometer. The crystalline structures of Al-MCM-41 and HPA/C were determined by X-ray diffraction (XRD) using a Shimadzu XD-D1 diffractometer and Ni-filtered Cu Kα radiation.

Sample acidity was determined by temperature programmed desorption (TPD) of NH_3 preadsorbed at 373 K. Samples (200 mg) were treated in He (60 cm^3/min) at 773 K for 2 h and then exposed to a 1% NH_3/He stream for 40 min at 373 K. Weakly adsorbed NH_3 was removed by flowing He at 373 K during 2 h. Temperature was then increased at 10 K/min and the NH_3 concentration in the effluent was measured by mass spectrometry in a Baltzers Omnistar unit.

The nature of surface acid sites was determined by infrared spectroscopy (IR) using pyridine as probe molecule and a Shimadzu FTIR-8101M spectrophotometer. Sample wafers were formed by pressing 20–40 mg of the catalyst at 5 tons/cm^2 and transferred to a sample holder made of quartz. All the samples were initially outgassed at 723 K for 4 h and then a background spectrum was recorded after cooling the sample at room temperature. Spectra were recorded at room temperature, after admission of pyridine, adsorption at room temperature and sequential evacuation at 298, 423, 573, and 723 K.

The gas-phase acylation of phenol (Merck, >99%) with acetic acid (Merck, 99.5%) was carried out in a fixed bed, continuous-flow reactor at 553 K and 101.3 kPa. Samples were sieved to retain particles with 0.35–0.42 mm diameter for catalytic measurements and pretreated in air at 773 K for 2 h before reaction. Phenol (P) and acetic acid (AA) were introduced (P/AA = 1) via a syringe pump and vaporized into flowing N_2 to give a N_2/(P + AA) ratio of 45. Standard catalytic tests were conducted at a contact time (W/F_P^0) of 146 g h/mol and gas-hour space velocity (GHSV) of 235 cm^3 STP/g min. The exit gases were analyzed on-line using a Hewlett–Packard 6850 chromatograph equipped with an Innowax column and a flame ionization detector. Data were collected every 25 min for about 6 h. Main products of phenol acylation with acetic acid were phenyl acetate (PA), *ortho*-hydroxyacetophenone (*o*-HAP), and para-hydroxyacetophenone (*p*-HAP). Phenol conversion (X_P, mol of phenol reacted/mol of phenol fed) was calculated as: $X_P = \Sigma Y_i/(\Sigma Y_i + Y_P)$, where ΣY_i is the molar fraction of products formed from phenol and Y_P is the outlet molar fraction of phenol. The selectivity to product i (S_i, mol of product i/mol of phenol reacted) was determined as: S_i (%) = $[Y_i/\Sigma Y_i]100$. Product yields (η_i, mol of product i/mol of phenol fed) were calculated as $\eta_i = S_i\, X_P$.

Gas-phase rearrangement of PA and the reaction between PA and P were studied using the same reaction unit and chromatographic analysis as those described above for acylation of P with AA. The reaction conditions for PA rearrangement were: T = 553 K, P = 101.3 kPa, P_{PA} = 0.638 kPa, W/F_{PA}^0 = 43.1 g h/mol; and for PA with P: T = 553 K, P = 101.3 kPa, $P_{PA} = P_P$ = 0.638 kPa, W/F_{o-HAP}^0 = 43.1 g h/mol.

3. Results and discussion

3.1. Catalyst characterization

The values of surface area and mean pore volume of the samples are given in Table 1. BET surface area of supported HPA/C was 390 m^2/g, significantly lower than that of carbon before impregnation (S_g = 1700 m^2/g). Bulky HPA molecules block the carbon micropore structure, as was confirmed by pore distribution measurements, thereby diminishing the surface

Table 1
Physical properties and acidity of the samples used in this work

Samples	Surface area, S_g (m^2/g)	Pore diameter, $\overline{d}_p$(Å)	TPD NH_3 (μmol/g)
ZSM-5	350	5.5	770
HPA/C	390	30	315
NaY	700	7.4	280
Al-MCM-41	925	30	340

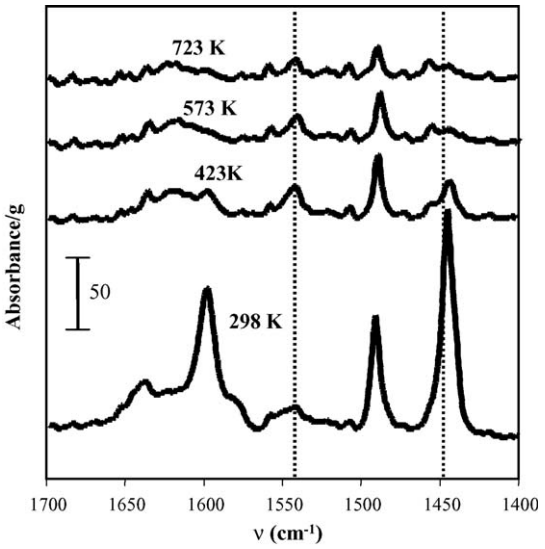

Fig. 1. IR spectra of pyridine adsorbed on zeolite ZSM5 at 298 K and evacuated at increasing temperatures. Doted lines indicate the presence of Lewis (1450 cm^{-1}) and Brönsted (1540 cm^{-1}) sites.

area and increasing the mean pore diameter (from 22 to 30 Å) of the support. X-ray diffraction pattern of Al-MCM-41 showed that this sample is well crystallized and exhibits a strong diffraction peak at 2.14° corresponding to 100 reflection, and two small peaks at 3.72° and 4.30° corresponding to 110 and 200 reflections, respectively. On the other hand, no crystalline HPA structure was detected on HPA/C, thereby indicating that the HPA phase is well dispersed on the carbon support.

Sample acid properties were probed by TPD of NH_3 preadsorbed at 373 K. The TPD profiles obtained for samples of Table 1 were reported in a previous work [11]. It was found that the evolved NH_3 from ZSM5 gave rise to a peak at 483–493 K and a broad band between 573 and 773 K while zeolite NaY desorbed NH_3 in a single TPD peak centered at about 480 K. The acid site strength of HPA/C was clearly higher as compared to the other samples, and showed a sharp NH_3 desorption peak at about 910 K, which accounted for the strong Brönsted acid sites present on this material. The NH_3 surface densities for acid sites were obtained by deconvolution and integration of TPD traces and are presented in Table 1. On a weight (770 μmol/g) or an areal (2.2 μmol/m^2) basis, the ZSM5 zeolite exhibited the highest surface acid density. For the other samples, the amount of evolved NH_3 was between 280 and 340 μmol/g.

Fig. 1 shows the IR spectra of adsorbed pyridine obtained on zeolite ZSM5 after admission of pyridine, adsorption at room temperature, and sequential evacuation at 298, 423, 573, and 723 K. The pyridine absorption bands at around 1540 cm^{-1} and between 1440 and 1460 cm^{-1} arise from pyridine adsorbed on Brönsted and Lewis acid sites, respectively, on zeolites [14–16] and Al-MCM-41 [17,18]. Fig. 1 shows that the spectrum collected following evacuation at 298 K contains broad absorption bands characteristics of the presence of physisorbed pyridine. Pyridine molecules interacting via H-bonding with weakly acidic surface OH groups (bands at 1446 and 1597 cm^{-1}) are removed after evacuation at 423 K and the resulting IR spectrum shows well defined absorption peaks. Similar IR characterization than that shown in Fig. 1 was performed for Al-MCM-41 and NaY samples. The density of Lewis and Brönsted acid sites were obtained by deconvolution and integration of pyridine absorption bands appearing at around 1450 and 1540 cm^{-1}, respectively. The evolution of the amount of pyridine adsorbed on Lewis and Brönsted sites as a function of the evacuation temperature on ZSM5, NaY, and Al-MCM-41 samples is shown in Fig. 2. Zeolite NaY did not contain Brönsted acid sites but exhibited the highest density of Lewis sites after evacuation at 423 K (525 area/g), and the IR band reflecting the adsorption of pyridine on Na Lewis sites appeared even after evacuation at 723 K. The amounts of pyridine adsorbed on Brönsted and Lewis sites of zeolite ZSM5 were similar following evacuation at 423 K (about 340 area/g) and 723 K (150–160 area/g). The significant amounts of pyridine present on ZSM5 after evacuation at high temperatures indicate that it contains strong Lewis and Brönsted acid sites. In agreement with the results obtained by TPD of NH_3, the amount of pyridine adsorbed on Al-MCM-41 was clearly lower as compared to zeolite ZSM5; moreover, Fig. 2 shows that pyridine was almost completely eliminated after evacuation at 723 K reflecting the moderate acidic character of mesoporous Al-MCM-41 sample. On the other hand, the relative Lewis/Brönsted site concentration determined after evacuation at 423 K was clearly higher on Al-MCM-41 (∼4.2) than on ZSM5 (∼1).

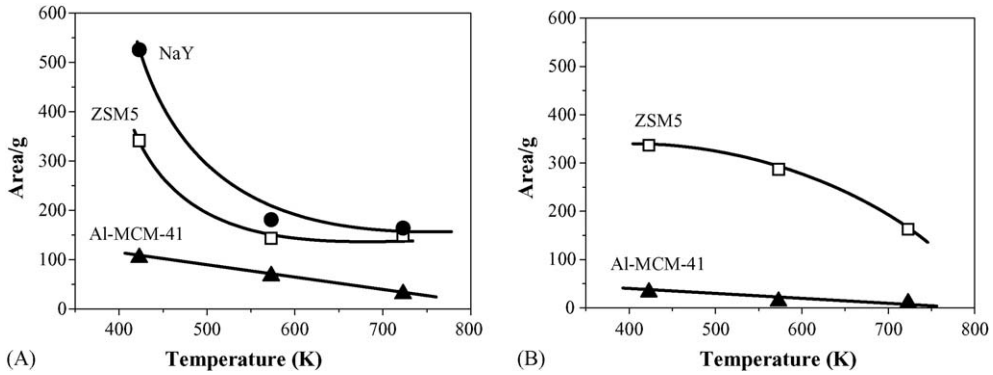

Fig. 2. IR spectra of adsorbed pyridine: evolution of Lewis (A) and Brönsted (B) peak intensities as a function of the evacuation temperature on ZSM5, NaY, and Al-MCM-41 samples.

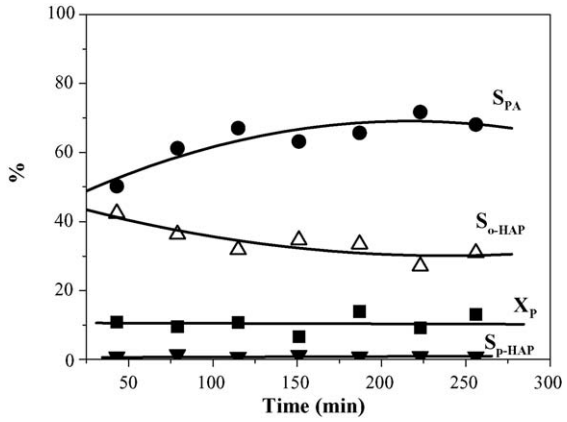

Fig. 3. Phenol conversion and product selectivities as a function of time on stream on Al-MCM-41 [553 K, 101.3 kPa total pressure, W/F_P^0 = 146 g h/mol, P/AA = 1, N_2/(P + AA) = 45].

3.2. Catalytic results

Samples of Table 1 were tested for the phenol/acetic acid reaction. Fig. 3 shows the evolution of phenol conversion (X_P) and product selectivities (S_i) as a function of time on Al-MCM-41 and typically illustrates the time-on-stream behavior of the catalysts during the reaction. Phenol conversion practically remained unmodified but the product selectivity significantly changed during the catalytic test. The PA selectivity increased with time on stream at expenses of the formation of *ortho*-HAP isomer. On the other hand, the formation of *o*-HAP compared to that of *p*-HAP was highly favored. Qualitatively, similar catalytic behavior on stream was observed for the other samples, excepting ZSM5. In fact, on ZSM5 not only X_P but also the product selectivities did not change with time on stream. Due to catalyst deactivation observed in Fig. 3, we decided to calculate the catalytic results by extrapolation of reactant and products concentration curves to zero time on stream. Then, X, S, and η reported here represent conversion, selectivity, and yield at $t = 0$, respectively.

Fig. 4 shows phenol conversion and product yields at zero time on stream as a function of contact time (W/F_P^0 = 25–200 mol/h g) on NaY and Al-MCM-41. In a previous paper [11], we showed the same type of curves obtained on HPA/C and ZSM5 samples. From the initial slopes of X_P versus W/F_P^0 curves we calculated the initial phenol conversion rates (r_P^0, mmol/h g) for all the catalysts; results are given in Table 2. The r_P^0 values followed the trend: ZSM5 > HPA/C > NaY > Al-MCM-41. Table 2 also compares the selectivities to PA and *o*-HAP obtained at similar phenol conversion (X_P = 15%); it is observed that the selectivity to *o*-HAP was clearly higher on ZSM5 and NaY (about 65% on both samples) than on Al-MCM-41 or HPA/C.

Initial formation rates of product i on NaY and Al-MCM-41 were calculated from the initial slopes of η_i versus W/F_P^0 curves in Fig. 4; results are shown in Table 2. Zeolite NaY formed PA and *o*-HAP directly from phenol, but r_{PA}^0 (0.77 mmol/h g) was clearly higher than r_{o-HAP}^0 (0.25 mmol/h g). PA yield increased with increasing W/F_P^0 on NaY but reaches a maximum value as it converts consecutively to *o*-HAP (Fig. 4A). Formation of *p*-HAP was not significant in the W/F_P^0 range studied. Qualitatively, similar behavior regarding the relative values of r_{PA}^0 and r_{o-HAP}^0, and the evolution of η_{PA} with contact time was observed on Al-MCM-41 (Fig. 4B). In a previous paper

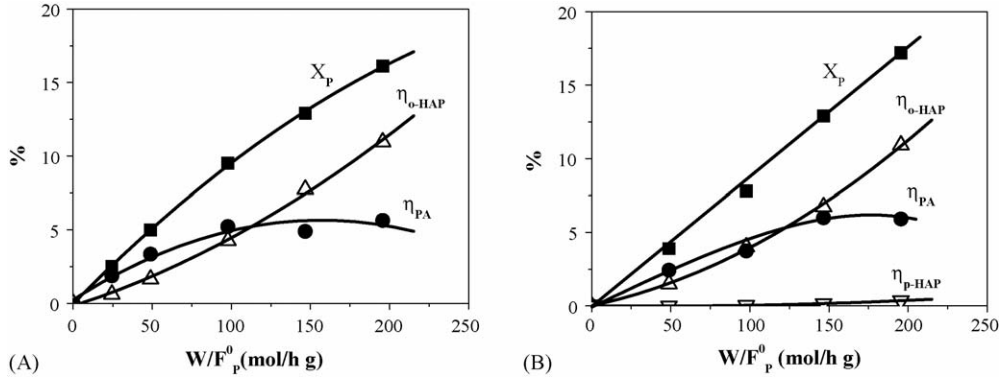

Fig. 4. Product yields and phenol conversion as a function of contact time on: (A) NaY; (B) Al-MCM-41 [553 K, 101.3 kPa total pressure, P/AA = 1].

Table 2
Catalytic results for the acylation of phenol with acetic acid

Catalyst	Phenol conversion rate, r_P^0 (mmol/h g)	Product formation rates		Selectivity (%)[a]	
		r_{o-HAP}^0 (mmol/h g)	r_{PA}^0 (mmol/h g)	S_{PA}	S_{o-HAP}
ZSM5	1.39	0.90	0.49	33	64
HPA/C	1.28	0	1.28	56	44
NaY	1.02	0.25	0.77	34	66
Al-MCM-41	0.80	0.30	0.50	43	54

T = 553 K, P/AA = 1, N_2/(P + AA) = 45.
[a] Determined at X_P = 15%.

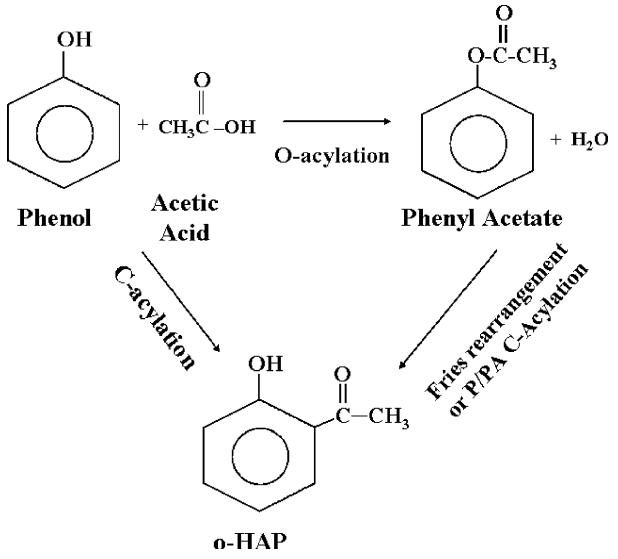

Fig. 5. Primary and secondary reaction pathways for the synthesis of *o*-HAP from phenol and acetic acid.

[11], we presented the η_i versus W/F^0_P curves obtained on HPA/C and ZSM5 samples; in Table 2, we show the initial product formation rates calculated from these curves. HPA/C formed initially only PA that was then consecutively converted to *o*-HAP. ZSM5 transformed phenol directly to both PA and *o*-HAP, but r^0_{o-HAP} (0.90 mmol/h g) was significantly higher than r^0_{PA} (0.49 mmol/h g), in contrast with the results obtained on NaY and Al-MCM-41 samples.

Based on the effect of contact time on product distribution shown in Fig. 4 and previous work [11,19], the primary and secondary reaction pathways involved in the synthesis of *o*-HAP from phenol and acetic acid are described in Fig. 5. According to Fig. 5, *o*-HAP is formed from phenol and AA via two parallel pathways: (i) the direct C-acylation of phenol; (ii) the O-acylation of phenol forming the PA intermediate which is then transformed to *o*-HAP via intramolecular Fries rearrangement or intermolecular phenol/PA C-acylation. Our results show that the relative rate of the different pathways involved in Fig. 5 greatly depends on the solid acid employed. In fact, zeolite ZSM5 that contains both strong Brönsted and Lewis sites exhibits the highest initial phenol conversion rate (Table 2) and is the only catalyst to promote the C-acylation of phenol to *o*-HAP at higher rates than the O-acylation of phenol to PA. HPA/C that contains only very strong Brönsted acid sites is not active for the C-acylation of phenol with AA and forms *o*-HAP exclusively via a secondary reaction pathway that requires the formation of PA intermediate. Finally, on both Lewis acid NaY and Al-MCM-41 of moderate Lewis and Brönsted acidity the rate of C-acylation of phenol to *o*-HAP is significantly lower than that of O-acylation of phenol to PA.

In order to obtain more insight on the relationship between the nature and strength of surface acid sites and the reaction pathways leading from phenol to *o*-HAP in Fig. 5, we performed additional catalytic tests using different reactants. We studied first the conversion of acetic acid that is the reactant responsible for the generation of the acylating agent or acylium ion CH_3CO^+. The values obtained for acetic acid conversion at $t = 0$ are given in Table 3; main reaction product was acetone. The catalyst activity trend was: ZSM5 > HPA/C > NaY > Al-MCM-41, following the same order observed for the initial phenol conversion rate in Table 2. Generated electrophile CH_3CO^+ may then attack the phenol molecule either by electrophilic substitution of the *ortho*-hydrogen in the aromatic ring forming *o*-HAP or, alternatively, by O-acylation of the OH group producing PA as depicted in Fig. 6. Results in Table 2 shows that on HPA/C sample, which contains only surface Brönsted sites, phenol is initially converted exclusively to PA. This is explained by considering that on strong Brönsted acid sites of HPA-based catalysts the phenol molecule essentially interacts via the benzene ring [20], adopting a position parallel to the surface and favoring the attack of acylium ion mainly to the oxygen of phenol, as shown in Fig. 6A. In contrast with HPA/C, Lewis acidic NaY catalyzes the C-acylation of phenol to *o*-HAP. In Fig. 6B, it is represented the adsorption of phenol on Lewis acid centers, which occurs predominantly in vertical orientation [20,21], and allows the electrophilic attack of benzene ring in *ortho*-position, because stabilization of the *ortho*-isomer intermediate is favored as compared to the intermediate formation in *para*-position [19]. The density and strength of Lewis acid sites are similar in NaY and ZSM5 (Fig. 2A), but the *o*-HAP formation rate from C-acylation of phenol is clearly higher on ZSM5 than on NaY (Table 2). This is probably because zeolite ZSM5 is much more active than NaY for generating acylium ions from acetic acid (Table 3).

Table 3
Catalytic results obtained using as reactants acetic acid, phenyl acetate, or phenyl acetate + phenol

Catalyst	Reactants							
	Acetic acid[a]	Phenyl acetate[b]				Phenyl acetate + phenol[c]		
	X_{AA} (%)	X_{PA} (%)	$\eta_{o\text{-HAP}}$(%)	η_P (%)	W/F^0_{PA} (g h/mol)	X_{PA} (%)	$\eta_{o\text{-HAP}}$(%)	η_P(%)
ZSM5	8.8	66.0	4.2	61.8	43.1	65.0	58	7
HPA/C	8.0	46.0	25.3	20.7	8.6	–	–	–
NaY	4.2	50.0	0	45.0	43.1	40.0	0	40
Al-MCM-41	1.6	40.0	6.5	32.8	43.1	40.0	17	23

[a] $T = 553$ K, $P = 101.3$ kPa, $P_{AA} = 1.10$, $W/F^0_{AA} = 146$ g h/mol.
[b] $T = 553$ K, $P = 101.3$ kPa, $P_{PA} = 0.683$ kPA.
[c] $T = 553$ K, $P = 101.3$ kPa, $P_{PA} = P_P = 0.683$ kPa, $W/F^0_{PA} = 43.1$ g h/mol.

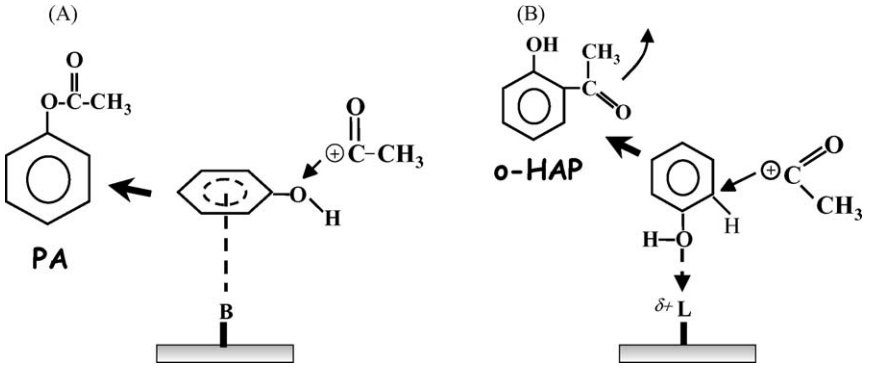

Fig. 6. Attack of the acylium ion to phenol to form (A) PA and (B) *o*-HAP on Brönsted and Lewis acid sites, respectively.

PA is an intermediate compound that is consecutively transformed to *o*-HPA on all the samples (see Fig. 4 for NaY and Al-MCM-41), either by intramolecular Fries rearrangement or by its decomposition and consecutive phenol acylation. In order to elucidate the mechanism of PA transformation to *o*-HAP on our catalysts, we studied both reaction pathways by feeding PA alone or together with phenol. Results are given in Table 3. When fed alone, PA may be converted on solid acids via two parallel reactions (Fig. 7): (i) Fries rearrangement of PA to *o*-HAP which involves the intramolecular migration of the acyl group to *ortho*-position of the aromatic ring; (ii) decomposition to phenol forming simultaneously ketene. Results in Table 3 show that when PA is the exclusive reactant, samples NaY, Al-MCM-41, and ZSM5 form mainly phenol and negligible amounts of *o*-HAP, thereby indicating that the Fries rearrangement mechanism is not promoted on these samples. In contrast, HPA/C is very active for the PA conversion reaction and forms predominantly *o*-HAP. From these results, we conclude that the Fries rearrangement of PA to *o*-HAP requires the presence of very strong Brönsted acid sites on the catalyst surface.

Finally, we studied the formation of *o*-HAP by cofeeding PA and phenol on samples Al-MCM-41, NaY, and ZSM5. As shown in Table 3, zeolite ZSM5 was active and selective for transforming PA to *o*-HAP via intermolecular P/PA acylation; Al-MCM-41 was also active for this reaction, but the *o*-HAP selectivity was clearly lower as compared to ZSM5. In contrast, NaY was inactive for *o*-HAP formation. This later result shows that Lewis acid NaY cannot form any acylating agent to attack phenol in *ortho*-position when PA and phenol compose the reactant mixture. However, zeolite NaY efficiently catalyzes the conversion of PA to *o*-HAP during the acylation of phenol with AA (Fig. 4A) because it is active for generating the acylating agent from AA (Table 3).

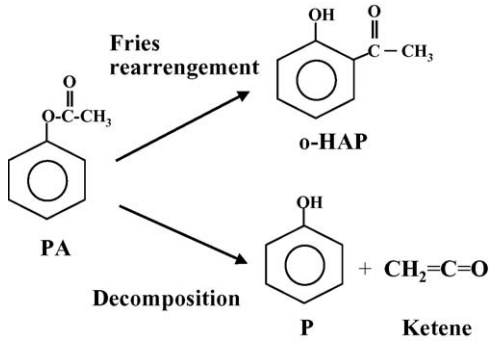

Fig. 7. Phenyl acetate conversion reactions on solid acids.

4. Conclusions

The reaction between phenol and acetic acid forms *o*-HAP either directly by C-acylation of phenol or indirectly from phenyl acetate that is initially produced by O-acylation of phenol. Samples containing only Lewis acidity (NaY), or both Brönsted and Lewis acid sites (Al-MCM-41, ZSM5) produce directly *o*-HAP from phenol because C-acylation of phenol is promoted on Lewis acid sites. However, the initial *o*-HAP formation rate is clearly higher on ZSM5 than on NaY and Al-MCM-41, because ZSM5 contains a higher density of strong Brönsted and Lewis acid sites, which catalyze more efficiently the generation of acylating agent CH_3CO^+ from acetic acid. Sample HPA/C containing only strong Brönsted acid sites is not active for the C-acylation of phenol.

Formation of phenyl acetate by O-acylation of phenol is easily promoted on solid acids containing Lewis or Brönsted acidity, but the consecutive reaction pathway leading from phenyl acetate to *o*-HAP greatly depend on the nature of surface acid sites. The Fries rearrangement of phenyl acetate to *o*-HAP occurs only on samples containing very strong Brönsted sites, such as HPA/C, while samples containing both Brönsted and Lewis acid sites, such as Al-MCM-41 and ZSM5, promote essentially the formation of *o*-HAP by intermolecular phenol/phenyl acetate acylation.

Acknowledgements

We thank the Universidad Nacional del Litoral (UNL), Consejo Nacional de Investigaciones Científicas y Técnicas (CONICET), and Agencia Nacional de Promoción Científica y Tecnológica (ANPCyT), Argentina, for the financial support of this work.

References

[1] I. Uwaydah, M. Aslam, C. Brown, S. Fitzhenry, J. McDonough, US Patent 5696274, 1997.

[2] M.J. Climent, A. Corma, S. Iborra, J. Primo, J. Catal. 151 (1995) 60.
[3] M.T. Drexler, M.D. Amiridis, J. Catal. 214 (2003) 136.
[4] J. Fritch, O. Fruchey, T. Horlenko, US Patent 4954652, Hoechst Celanese Corporation, 1990.
[5] J. Mueller, W. Wiersdorff, W. Kirschenlohr, G. Schwantje, US Patent 4508924, BASF, 1985.
[6] G.N. Mott, US Patent 4607125, Celanese Corporation, 1986.
[7] V. Pouilloux, J.-P. Bodibo, I. Neves, M. Gubelnann, G. Perot, M. Guisnet, in: M. Guisnet, et al. (Eds.), Heterogeneous Catalysis and Fine Chemicals II, Elsevier, Amsterdam, 1991, p. 513.
[8] V. Borzatta, G. Busca, E. Poluzzi, V. Roseetti, M. Trombetta, A. Vaccari, Appl. Catal. A: Gen. 257 (2004) 85.
[9] F. Jayat, M. Guisnet, M. Goldwasser, G. Giannetto, Stud. Surf. Sci. Catal. 105 (1997) 1149.
[10] Y.V. Subba Rao, S.J. Kulkarni, M. Subrahmanyam, A.V. Rama Rao, Appl. Catal. A: Gen. 133 (1995) L1.
[11] C.L. Padró, C.R. Apesteguía, J. Catal. 226 (2004) 308.
[12] C.L. Padró, C.R. Apesteguía, Catal. Today 107–108 (2005) 258.
[13] K.J. Edler, J.W. White, Chem. Mater. 9 (1997) 1226.
[14] E.P. Parry, J. Catal. 2 (1963) 371.
[15] J.W. Ward, J. Catal. 10 (1968) 34.
[16] H. Knözinger, Adv. Catal. 25 (1976) 184.
[17] J. Wang, L. Huang, H. Chen, Q. Li, Catal. Lett. 55 (1998) 157.
[18] A. Sakthivel, S.E. Dapurkar, N.M. Gupta, S.K. Kulshreshtha, P. Selvam, Microporous Mesoporous Mater. 65 (2003) 177.
[19] I. Neves, F. Jayat, P. Magnoux, G. Perot, F.R. Ribeiro, M. Gubelman, M. Guisnet, J. Mol. Catal. 93 (1994) 169.
[20] K.V.R. Chary, K. Ramesh, G. Vidyasagar, V.V. Rao, J. Mol. Catal. A: Chem. 198 (2003) 195.
[21] K. Tanabe, T. Nishizaki, in: G.C. Bond, P.B. Wells, F.C. Tompkins (Eds.), Proceedings of the Sixth International Conference on Catalysis, vol. 2, The Chemical Society, London, (1977), p. 863.